Advances in Nano Research, *Vol. 10, No. 2 (2021) 115-128*
DOI: https://doi.org/10.12989/anr.2021.10.2.115

Free vibration of electro-magneto-thermo sandwich Timoshenko beam made of porous core and GPLRC

Mohammad Safari, Mehdi Mohammadimehr* and Hossein Ashrafi

Department of Solid Mechanics, Faculty of Mechanical Engineering, University of Kashan, Ghotb Ravandi Blvd., Kashan, Iran

(*Received March 10, 2020, Revised November 15, 2020, Accepted November 20, 2020*)

Abstract. In this article, free vibration behavior of electro-magneto-thermo sandwich Timoshenko beam made of porous core and Graphene Platelet Reinforced Composite (GPLRC) in a thermal environment is investigated. The governing equations of motion are derived by using the modified strain gradient theory for micro structures and Hamilton's principle. The magneto electro are under linear function along the thickness that contains magnetic and electric constant potentials and a cosine function. The effects of material length scale parameters, temperature change, various distributions of porous, different distributions of graphene platelets and thickness ratio on the natural frequency of Timoshenko beam are analyzed. The results show that an increase in aspect ratio, the temperature change, and the thickness of GPL leads to reduce the natural frequency; while vice versa for porous coefficient, volume fractions and length of GPL. Moreover, the effect of different size-dependent theories such as CT, MCST and MSGT on the natural frequency is investigated. It reveals that MSGT and CT have most and lowest values of natural frequency, respectively, because MSGT leads to increase the stiffness of micro Timoshenko sandwich beam by considering three material length scale parameters. It is seen that by increasing porosity coefficient, the natural frequency increases because both stiffness and mass matrices decreases, but the effect of reduction of mass matrix is more than stiffness matrix. Considering the piezo magneto-electric layers lead to enhance the stiffness of a micro beam, thus the natural frequency increases. It can be seen that with increasing of the value of W_{GPL}, the stiffness of microbeam increases. As a result, the value of natural frequency enhances. It is shown that in h_c/h = 0.7, the natural frequency for W_{GPL} = 0.05 is 8% and 14% less than its for W_{GPL} = 0.06 and W_{GPL} = 0.07, respectively. The results show that with an increment in the length and width of GPLs, the natural frequency increases because the stiffness of micro structures enhances and vice versa for thickness of GPLs. It can be seen that the natural frequency for a_{GPL} = 25 μm and h_c/h = 0.6 is 0.3% and 1% more than the one for a_{GPL} = 5 μm and a_{GPL} = 1 μm, respectively.

Keywords: free vibration; Timoshenko sandwich beam; piezo-magnetic; piezo-electric; graphene platelets; temperature dependent material properties

1. Introduction

Engineering systems combined with a cored sandwich between face sheets are frequently used in various industries in the role of load-carrying members according to their high stiffness to weight ratio. Thus, scientists have been studying comprehensively to analyze the behavior of this structure in researches. In this study, this kind of subjects are taken to investigate a sandwich Timoshenko beam made of porous core and Graphene Platelet Reinforced Composite (GPLRC).

1.1 Dynamic, vibration and buckling of porous structures

Porous substance, like metal foams, are being used as advanced materials. This kind of materials is used in aerospace engineering, automobile industry and some engineering structures. The most important factors that are attracting scientists and engineers' attention to porous materials are their efficient capacity of energy loss, low specific weight, low thermal and electrical conductivity and recyclability (Gibson and Ashby 1997). Sandwich porous plates and beams are weight-efficient structures which have three different parts: Two thin face sheets that afford stiffness, a thick core that tolerates shear loads which provides a heat diffuser and also a vibration damper. Since last few years, sandwich porous beams' dynamic and static properties have been investigated by different experimental analyses and theoretical researches (Wadley *et al*. 2003, Crupi and Montanini 2007, Tagarielli *et al*. 2007, Qin and Wang 2009, Shahdin *et al*. 2009). Magnuca-blandzi (2011) introduced a mathematical model for simply-supported sandwich porous plate using the principle of stationary of the total potential energy. Chen *et al.* (2016b) obtained forced and free vibration specifications of FG porous beams with non-uniform porosity distribution. Mass density and elastic moduli were considered nonlinear along the vertical direction. They concluded that beam with higher porosity ratio has more considerable dynamic deflections than it's correlated with a smaller porosity ratio. They also showed that by increasing slenderness ratio, the natural frequency diminishes meaningfully and the dynamic deflection increase significantly. Grygorowicz *et al.* (2015) analyzed

*Corresponding author, Ph.D., Associate Professor,
E-mail: mmohammadimehr@kashanu.ac.ir;
mmohammadimehr@gmail.com

ISSN: 2287-237X (Print), 2287-2388 (Online)

the buckling analysis of a sandwich three-layered beam with a metal foam core, and the numerical analysis was carried out in ANSYS using a linear elastic buckling model.

1.2 Dynamic behavior of composites and sandwich structures in thermal environment

Heretofore, several dynamic types of research have been accomplished by researchers on composites and sandwich beams. Mohammadimehr and Mostafavifar (2016) analyzed free vibration of a sandwich plate with Functionally Graded Carbon Nanotubes (FG-CNT) reinforced composite and a transversely flexible core using Strain Gradient Theory (SGT). They used temperature-dependent materials, and their model was subjected to a magnetic field and made of temperature-dependent material. They investigated that the frequency of sandwich carbon nanotube plate with X distribution is higher than other kinds of distributions and introducing the material length scale parameters and assuming the size effects increases the natural frequency of the sandwich plate. Mohammadimehr *et al*. (2015a) analyzed the free vibration analysis of a viscoelastic double-bonded Carbon Nanotube (CNT) reinforced composites. Their results were investigated by using a Sinusoidal Shear Deformation Theory (SSDT). They revealed that the natural frequency of their structure has a reverse relevance with damping coefficient while the natural frequency has direct effect using the material length scale parameters. Wu *et al*. (2015) investigated elastic buckling and free vibration of sandwich beam with rigid core and FG-CNT reinforced composite using Timoshenko beam theory. Their numerical outcomes showed that slenderness coefficient, CNT volume fraction, and boundary conditions have a notable effect on the natural frequencies. They also showed that with an increase in axial load, the natural frequency of the sandwich beam was reduced. Mohammadimehr *et al*. (2016) used Modified Strain Gradient Theory (MSGT) and Third-order Shear Deformation Theory (TSDT) to investigate free vibration, bending and buckling analyses of a micro composite plate reinforced by Functionally Graded Single-Walled Carbon Nanotube (FG-SWCNT) in the hydro-thermal environments. They showed that the natural frequency and critical buckling load for modified couple stress theory (MCST) and Classic Theory (CT) are less than the MSGT. They also claimed that the material length scale parameters increase the rigidity of the beam. Zhou *et al*. (2016) studied carbon fiber reinforced composites using finite element method. They showed that the CNT lead to increase composite strength because adding CNTs into the matrix, the conjunction capacity of the matrix is improved to the delaminating crack proliferation. They also revealed that CNTs with high volume values are better than lower values. Guo and Zhang (2016) investigated chaotic dynamic and nonlinear oscillation of a thin composite plate with CNTs subjected to parametric and forcing excitation based on Mori-Tanaka method. They obtained the complex response of nonlinear vibration and found that both chaotic and periodic motion become evident for their model. Hosseini and Jamalpoor (2015) studied the dynamic analysis of a double-FG viscoelastic nanoplate resting on Pasternak foundation in a temperature-dependent environment assuming surface influences. Their obtained results showed that the natural frequency is dramatically affected by residual surface stress and nonlocal parameters, half wave number and Pasternak flexible foundation. They also showed that an increase in the temperature change leads to decrease in the natural frequency. Mohammadimehr *et al*. (2018) presented bending, buckling and free vibration analyses of carbon nanotube reinforced composite beams and experimental tensile test to obtain the mechanical properties of nanocomposite. Ninh (2018) analyzed nonlinear thermal torsional post-buckling of carbon nanotube-reinforced composite cylindrical shell surrounded by elastic medium with piezoelectric actuator layers. He considered both uniform and functionally graded distribution of reinforcements through the thickness of the shells. Elastic modulus of a hybrid aluminium matrix nanocomposite (HAMNC) reinforced with SiC nano-particles and silicon carbide (SiC) whiskers are investigated by Chen *et al*. (2018) using a new multi-scale analytical model to calculate the effective elastic modulus of the HAMNC. Electro-thermo-mechanical vibration of nano-composite cylindrical shells with an internal fluid flow investigated by Ninh *et al*. (2019) based on geometrical nonlinearity in classical thin shell theory (CLT). They considered both uniform and functionally graded CNTs. Zeverdejani and Beni (2020) presented the effect of laminate configuration on the free vibration/buckling analyses of FG graphene/PMMA composites. Si Tayeb *et al*. (2020) considered the mechanical buckling of FG-CNTs reinforced composite plate with parabolic distribution using Hamilton's energy principle. Noroozi *et al*. (2020) depicted the torsional vibration analysis of bi-directional FG nano-cone with arbitrary cross-section based on nonlocal strain gradient elasticity. Tien *et al*. (2020) obtained nonlinear vibration analysis of functionally graded carbon nanotube-reinforced polymer plate resting on elastic foundations under electro-thermo-mechanical loads using an analytical approach. The dynamical responses such as phase plane graphs, time history and Poincaré formula are investigated in their study. The effects of non-uniform elastic foundation on non-linear thermal dynamics of the simply supported plate reinforced by Functionally Graded (FG) Graphene Nanoplatelets (GNPs) are investigated by Hoang *et al*. (2020a) using Selvadurai method. Babaeeian and Mohammadimehr (2020) investigated the time elapsed effect on residual stress measurement in a composite plate by DIC method.

1.3 Piezoelectric components in sandwich beams

The Magneto-Electro-Elastic (MEE) structures have been noticed in current decades. Some researchers have focused on beams with piezoelectric face layers. Zenkour and Arefi (2017) considered forward nonlocal bending and vibration analysis of a Functionally Graded Piezoelectric (FGP) nanosheet on a visco-Pasternak foundation. Rajabi and Mohammadimehr (2019) analyzed hydro-thermo-mechanical buckling of isotropic/orthotropic cored micro sandwich plate with piezoelectric/polymetric face layer.

They adopted the First Shear Deformation Theory (FSDT) for the micro sandwich plate. It was revealed from outcomes that nondimensional critical buckling of carbon nanotube is higher than of for boron nitride nanotube. Rafiee *et al*. (2013) studied free vibration analysis of FG-CNT reinforced composite beam with piezoelectric layers under an applied voltage and temperature change based on Euler-Bernoulli beam theory, physical natural surface concept, and von Karman geometric nonlinearity. They used multiple time scales method to obtain parameters related to nonlinear vibration of both ends clamped beam. Mohammadimehr *et al*. (2015b) studied electro-elastic solution of a sandwich plate on the Pasternak foundation using TSDT. They also considered FG core and composite and piezoelectric face sheets. An electro-thermo-mechanical vibration of Functionally Graded Carbon Nanotube-Reinforced Composite (FG-CNTRC) cylindrical shells by an analytical approach is studied by Ninh and Bich (2018). They used uniform and functionally graded CNTs to reinforce through the thickness of the shell. Ebrahimi *et al*. (2020) illustrated the dynamic characteristics of hygro-magneto-thermo-electrical nanobeam with non-ideal boundary conditions. Wang *et al*. (2020) investigated an engineered self-supported dendrite-free composite anode and electrocatalytic cathode using 3D double-carbon hosts for advanced Li-SeS_2 batteries.

1.4 Dynamic behavior of graphene platelets

Graphene platelets is a two-dimensional carbon atoms' monolayer. Properties and features of graphene platelets are considerable. Graphene platelets has comparable Young's modulus and tensile strength compare to CNTs. One of the advantages of this material is the abundance of it in nature which makes it cheaper when combined in large scales. In recent years, many studies have been done on graphene platelets by researchers. Wu *et al*. (2017) analyzed dynamic instability of multilayer nanocomposite FG beams reinforced with graphene nanoplates (GPLs) in a thermal environment. The graphene weight fraction was considered to be constant in each layer and vary across the beam thickness. They also discussed thermal buckling and free vibration analysis of the beam. Their results showed that the natural frequency increases by distributing more GPLs near the bottom and top surfaces. Bahaadini and Saidi (2018) studied aeroelastic analysis of FG rotating blades reinforced with graphene nanoplates in supersonic flow. They assumed both uniformly and non-uniformly distributions along the beam thickness direction. The aerodynamic pressure was considered in accordance with the quasi-steady supersonic piston theory. Their results showed that by adding GPL to the matrix, the natural frequency of the composite blade increases. Barati and Shahverdi (2019) discussed forced vibration of shear deformable reinforced nanocomposite graphene face sheets in a thermal environment by using higher-order refined beam element and Finite Element (FE) theory. They assumed the distributions of GPL as nonlinear, uniform and linear. Their results revealed that the effects of GPL weighs fraction, temperature change, and GPL distribution affect the dynamic deflection. Shen *et al*. (2017) analyzed the vibration of FG laminated graphene beams resting on elastic foundation in thermal environments. Their equations of motion were derived according to Von Karman strain displacement formulations and a higher-order shear deformation beam theory. Their outcomes showed that graphene distributions could affect the vibration and stiffness parameters of graphene reinforced composites and the best distribution of graphene, which can reach the highest frequencies is FG-X symmetric distribution. Gao *et al*. (2018) represented mesophase pitch-based carbon foams as sound absorbers in acoustics fields. Nonlinear dynamics analysis of imperfect nanocomposite circular cylindrical shells with internal and external fluid flow and spinning annular is studied by Ninh *et al*. (2019) using higher order shear deformation shell theory. Zhao *et al*. (2019) reported the effects of three iron ores with different structures as catalytic beds on the distribution of co-pyrolysis products.

Nonlinear dynamics of functionally graded graphene nanoplatelet resting on elastic foundation reinforced polymer doubly-curved shallow shells are studied by Hoang *et al*. (2020b) using a micromechanical model. An experiment concerning regulation under coal pyrolysis, with iron ore as a catalytic bed, optimization of carbon deposition in spent samples and integration of multiple similar reaction factors between the pyrolysis of experimental models and volatile decomposition-carbon deposition is considered by Zhao *et al*. (2020) to reach the aforementioned goals.

According to the aforesaid researches, the free vibration analysis of a sandwich Timoshenko beam has been developed and investigated by some researchers, but no literature has been reported for the free vibration analysis of a micro sandwich Timoshenko beam made of porous core and facesheets reinforced by various distributions of GPLs under magneto-electro-thermo-mechanical loadings based on modified strain gradient theory. Also, it can be stated that investigating simultaneously porous core, various distributions of GPLs, piezo-magnetic, piezo-electric, three material length scale parameters can be the novelty of this research. The governing equations of motion are derived by using the strain gradient theory for a micro-structures and Hamilton's principle. The magneto electro face sheets are subjected a linear function along the thickness that contains magnetic and electric constant potentials and a cosine function. The effects of material length scale parameters, temperature change, various distributions of porous and thickness ratio on Timoshenko beam's natural frequency are investigated. The results of this research in the future work can be used to control the vibration amplitude of a micro beam in forced vibration by employing sensor and actuator in facesheets layers.

2. Modeling and formulation of problem

Fig. 1 shows a sandwich porous beam of length L and width b. The total thickness is $h = h_c + h_{p_1} + h_{p_2}$, where h_c indicates the thickness of the core and $h_{p_1}$and h_{p_2} are the thickness of top and bottom layers, respectively. The

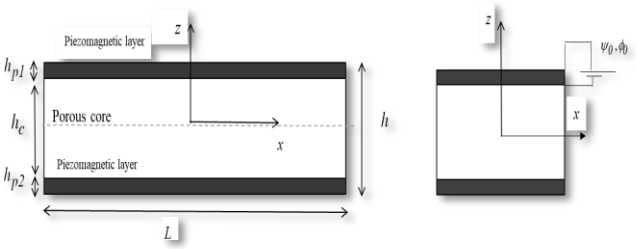

Fig. 1 A sandwich Timoshenko beam made of porous core and graphene piezo magneto-electric layers

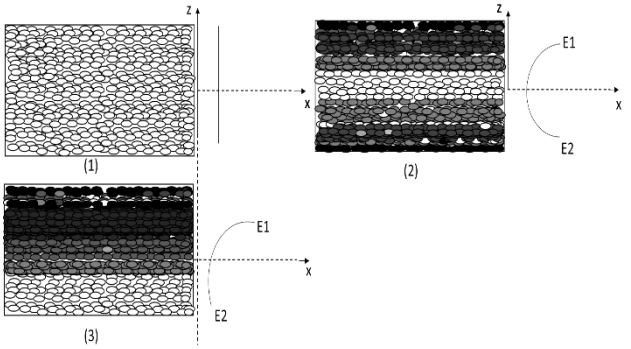

Fig. 2 Various distributions of porous core

piezo magnetoelectric face sheets are considered to be completely connected to the core. The *x-z* Cartesian coordinate system is shown in Fig. 1.

2.1 Porous core distributions and material properties

The density, Young's and shear moduli of porous core are considered as non-uniform and uniform distributions according to Fig. 2. Eqs. (1)-(3) are shown Young's modulus and density formulations for distribution 1, distribution 2 and distribution 3 of porous core, respectively (Chen *et al*. 2015).

$$\begin{cases} E(z) = E_1(1 - e_0\beta) \\ \rho(z) = \rho_1\sqrt{1 - e_0\beta} \\ G(z) = G_1(1 - e_0\beta) \end{cases} \tag{1}$$

$$\begin{cases} E(z) = E_1(1 - e_0\cos(\pi\lambda)) \\ \rho(z) = \rho_1(1 - e_m\cos(\pi\lambda)) \\ G(z) = G_1(1 - e_0\cos(\pi\lambda)) \end{cases} \tag{2}$$

$$\begin{cases} E(z) = E_1(1 - e_0\cos\left(\dfrac{\pi\lambda}{2} + \dfrac{\pi}{4}\right)) \\ \rho(z) = \rho_1(1 - e_m\cos\left(\dfrac{\pi\lambda}{2} + \dfrac{\pi}{4}\right)) \\ G(z) = G_1(1 - e_0\cos\left(\dfrac{\pi\lambda}{2} + \dfrac{\pi}{4}\right)) \end{cases} \tag{3}$$

where the maximum and minimum values of Young's modulus for non-uniform porosity distributions are represented as $E_1$and E_2, respectively, the corresponding values of mass density and shear modulus are denoted as ρ_i and G_i (i = 1, 2), and the porosity coefficient is defined as e_0. The mechanical property of an open-cell metal foam (Chen *et al*. 2016a, b) and porous characteristic can be considered as

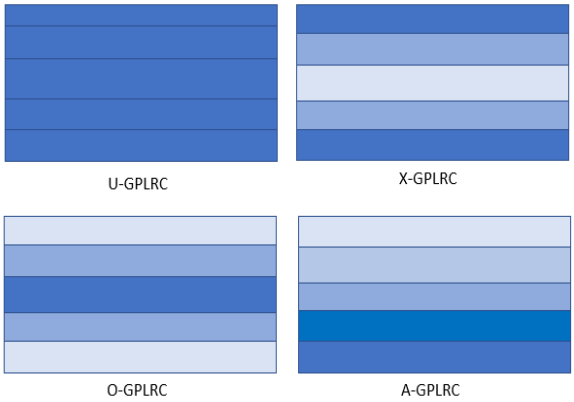

Fig. 3 Various distributions of graphene platelets microbeam

$$\frac{E_2}{E_1} = \left(\frac{\rho_2}{\rho_1}\right)^2 \tag{4}$$

$$e_m = 1 - \frac{\rho_2}{\rho_1} = 1 - \sqrt{\frac{E_2}{E_1}}, \qquad 0 \le e_m < 1 \tag{5}$$

$$e_0 = 1 - \frac{E_2}{E_1} = 1 - \frac{G_2}{G_1} = 1 - (1 - e_m)^2 \qquad 0 \le e_0 < 1 \tag{6}$$

and $\lambda = \frac{z}{h_c}(-\frac{h_c}{2} \le z \le \frac{h_c}{2})$. e_0 is a principle value for describing porosity values and e_m is obtained by using mechanical features of an open-cell metal foam. It should be noticed that e_m = e_0 = 1 can be attained when all material property contents are decreased to zero whereas e_m = e_0 = 0 shows that no hole is in the core.

As it is obvious in Fig. 2, the material properties of the sandwich porous core with uniform distribution does not change along the vertical direction. In uniform porosity distribution relations in Eq. (2), according to basis of the equivalent mass of sandwich prose beams, the coefficient β is explored as

$$\beta = \frac{1}{e_0} - \frac{1}{e_0}\left[\frac{2}{\pi}\sqrt{1 - e_0} - \frac{2}{\pi} + 1\right]^2 \tag{7}$$

2.2 Various distributions of graphene platelets

Face sheets layers for the sandwich beam are contained of piezo magnetoelectric materials reinforced by GPL. Various distribution models of GPLs along the vertical direction such as *U-GPLRC, X-GPLRC, O-GPLRC* and *A-GPLRC* are shown in Fig. 3. By using the four distribution models of GPLs, the volume fractions V_{GPL} along the thickness of the beam can be derived (Wu *et al*. 2017, Barati and Shahverdi 2019) as follows

$$V_{GPL}^{(k)}=\begin{cases}V_{GPL}^{*}U-GPLRC\\ 2V_{GPL}^{*}|2k-N_L-1|/N_LX-GPLRC\\ 2V_{GPL}^{*}(1-|2k-N_L-1|)/N_LO-GPLRC\\ V_{GPL}^{*}|2k-1|/N_LA-GPLRC\end{cases} \quad (8)$$

in which

$$V_{GPL}^{*}=\frac{W_{GPL}}{W_{GPL}+(\frac{\rho_{GPL}}{\rho_m})(1-W_{GPL})} \quad (9)$$

where ρ_m and ρ_{GPL} are density of polymer matrix and graphene platelets, respectively, and W_{GPL} is the weigh fraction of graphene platelets. Also, according to the Extended Mixture Rule (EMR) for shear modulus, Poisson's ratio and density and Halphin-Tsai for Young's modulus are introduced as follows

$$\begin{cases}\rho=V_{GPL}\rho_{GPL}+V_m\rho_m\\ \nu=V_{GPL}\nu_{GPL}+V_m\nu_m\\ E=\frac{3}{8}\frac{1+\xi_L\eta_LV_{GPL}}{1-\eta_LV_{GPL}}\times E_m+\frac{5}{8}\frac{1+\xi_T\eta_TV_{GPL}}{1-\eta_TV_{GPL}}\times E_m\\ V_m+V_{GPL}=1\\ \alpha=\alpha_{GPL}V_{GPL}+\alpha_mV_m\end{cases} \quad (10)$$

where parameters with index m and GPL correspond to matrix and graphene nanoplatelets, respectively. α_m and α_{GPL} are thermal coefficients that refer to matrix and GPLs, respectively. ν_m and ν_{GPL} are Poisson's modulus. Parameters ξ_L, ξ_T, η_L and η_T are defined as

$$\begin{cases}\eta_L=\frac{(E_{GPL}/E_m)-1}{(E_{GPL}/E_m)+\xi_L}\\ \eta_T=\frac{(E_{GPL}/E_m)-1}{(E_{GPL}/E_m)+\xi_T}\\ \xi_L=2(a_{GPL}/t_{GPL})\\ \xi_T=2(b_{GPL}/t_{GPL})\end{cases} \quad (11)$$

in which b_{GPL}, a_{GPL}, t_{GPL} indicate width, length and thickness of GPLs, respectively. E_m and E_{GPL} are Young's moduli of matrix and GPLs, respectively.

3. Displacement fields and theoretical formulation

In this section, the basic relations for analysis of a sandwich micro beam made of porous core and two piezo magnetoelectric layers in thermal environment are derived. Based on Timoshenko beam theory, the axial and transverse displacement fields are defined as follows

$$\begin{cases}u_x(x,z,t)=u_0(x,t)+z\theta_x(x,t)\\ w_z(x,z,t)=w_0(x,t)\end{cases} \quad (12)$$

u_0, w_0 and $\theta_x(x, t)$ are the values of axial, transverse displacements of mid-surface and rotation function, respectively. Using Eq. (12), the normal and shear strains (ε_{xx} and γ_{xz}) are obtained as

$$\begin{cases}\varepsilon_{xx}=\frac{\partial u_x(x,z,t)}{\partial x}=\frac{\partial u_0}{\partial x}+z\frac{\partial\theta_x}{\partial x}\\ \gamma_{xz}=\frac{\partial u_x(x,z,t)}{\partial z}+\frac{\partial u_z(x,z,t)}{\partial x}=\theta_x+\frac{\partial w_0}{\partial x}\end{cases} \quad (13)$$

Generally, strain-stress relations for combination of porous core composite beam and piezo magnetoelectric platelets are derived as follows

$$\sigma_{ij}=Q_{ijkl}(z).\varepsilon_{kl}+e_{mij}E_m-q_{mij}H_m-Q_{ijkl}\alpha_{ij}\Delta T \quad (14)$$

in which $Q_{ijkl}(z)$ indicates both stress components for a sandwich porous core and stiffness parameters of piezo magnetoelectric material, e_{mij} and q_{mij} are corresponding piezoelectric and magnetic coefficients, respectively. Moreover, H_m indicates magnetic field and E_m is electric field. The coefficients of temperature effects on both piezo magnetoelectric platelets and core is displayed by α_{ij}.

At first, magnetic and electric field should be defined before calculating stress equations. Magnetic and electric potentials are considered to be mixture of a parameter which is as linear function along the vertical axis z and a linear cosine function which satisfies boundary conditions as follows

$$\begin{cases}\psi(x,z,t)=\frac{2\bar{z}\psi_0}{h_p}-\psi(x,t)\cos\left(\frac{\pi\bar{z}}{h_p}\right)\\ \phi(x,z,t)=\frac{2\bar{z}\phi_0}{h_p}-\phi(x,t)\cos(\frac{\pi\bar{z}}{h_p})\end{cases} \quad (15a)$$

in which ϕ_0 and ψ_0 indicate applied magnetic and electric potentials, respectively. ϕ and ψ are magnetic and electric potential distributions, respectively. Variable $\bar{z}$ for top and bottom face sheet layers is expressed as follows

$$\begin{cases}\bar{z}_{top}=z+\frac{h}{2}+h_{p2}\\ \bar{z}_{bot}=z-\frac{h}{2}-h_{p1}\end{cases} \quad (15b)$$

According to the expressed magnetic and electric potentials in Eq. (15a), the parameters of magnetic and electric potentials are investigated as

$$\begin{cases}H_1=-\frac{\partial\phi(x,z,t)}{\partial x}=\frac{\partial\phi(x,t)}{\partial x}\cos(\frac{\pi\bar{z}}{h_p})\\ H_3=-\frac{\partial\phi(x,z,t)}{\partial z}=-\frac{2\phi_0}{h_p}-\phi(x,t)\frac{\pi}{h_p}\sin(\frac{\pi\bar{z}}{h_p})\end{cases} \quad (16)$$

$$\begin{cases}E_1=-\frac{\partial\psi(x,z,t)}{\partial x}=\frac{\partial\psi(x,t)}{\partial x}\cos(\frac{\pi\bar{z}}{h_p})\\ E_3=-\frac{\partial\psi(x,z,t)}{\partial z}=-\frac{2\psi_0}{h_p}-\psi(x,t)\frac{\pi}{h_p}\sin(\frac{\pi\bar{z}}{h_p})\end{cases} \quad (17)$$

in which h_{p1} and h_{p2} for top and bottom face sheet layers, respectively. The electric displacement and magnetic flux for a piezo magnetoelectric materials are shown as

$$D_i=e_{ijk}\varepsilon_{jk}+\eta_{ik}E_k+g_{ik}H_k \quad (18)$$

$$B_i=q_{ijk}\varepsilon_{jk}+g_{ik}E_k+\mu_{ik}H_k \quad (19)$$

Substituting Eqs. (13), (16), (17) into Eqs. (18) and (19)

yields non-zero electric displacement and magnetic flux as

$$\begin{cases} D_1 = e_{15}\left(\theta_x + \dfrac{\partial w_0}{\partial x}\right) + \eta_{11}\left(\dfrac{\partial \psi(x,t)}{\partial x} cos(\dfrac{\pi \bar{z}}{h_p})\right) \\ \qquad + g_{11}\left(\dfrac{\partial \phi(x,t)}{\partial x}\cos(\dfrac{\pi \bar{z}}{h_p})\right) \\ D_3 = e_{31}\left(\dfrac{\partial u_0}{\partial x} + z\dfrac{\partial \theta_x}{\partial x}\right) - \eta_{33}\left(\dfrac{2\psi_0}{h_p} + \psi(x,t)\dfrac{\pi}{h_p}\times\right. \\ \left.\sin(\dfrac{\pi \bar{z}}{h_p})\right) - g_{33}\left(+\dfrac{2\phi_0}{h_p} + \phi(x,t)\dfrac{\pi}{h_p}\sin(\dfrac{\pi \bar{z}}{h_p})\right) \end{cases} \tag{20}$$

$$\begin{cases} B_1 = q_{15}\left(\theta_x + \dfrac{\partial w_0}{\partial x}\right) + g_{11}\left(\dfrac{\partial \psi(x,t)}{\partial x}\cos(\dfrac{\pi \bar{z}}{h_p})\right) \\ \qquad + \mu_{11}\left(\dfrac{\partial \phi(x,t)}{\partial x}\cos(\dfrac{\pi \bar{z}}{h_p})\right) \\ B_3 = q_{31}\left(\dfrac{\partial u_0}{\partial x} + z\dfrac{\partial \theta_x}{\partial x}\right) - g_{33}\left(\dfrac{2\psi_0}{h_p} + \psi(x,t)\dfrac{\pi}{h_p}\times\right. \\ \left.\sin(\dfrac{\pi \bar{z}}{h_p})\right) - \mu_{33}\left(\dfrac{2\phi_0}{h_p} + \phi(x,t)\dfrac{\pi}{h_p}\sin(\dfrac{\pi \bar{z}}{h_p})\right) \end{cases} \tag{21}$$

According to Timoshenko beam theory, except σ_{xx} and τ_{xz}, all other stress components equal to zero. By substituting Eqs. (12), (16) and (17) into Eq. (13), the non-zero stress components can be obtained as

$$\sigma_{xx} = Q_{11}(z)\left(\frac{\partial u_0}{\partial x} + z\frac{\partial \theta_x}{\partial x}\right) + e_{31}\left(\frac{2\psi_0}{h_p} + \psi(x,t)\frac{\pi}{h_p}\times sin(\frac{\pi \bar{z}}{h_p})\right) + q_{13}\left(\frac{2\phi_0}{h_p} + \phi(x,t)\frac{\pi}{h_p}sin(\frac{\pi \bar{z}}{h_p})\right) - Q_{11}\alpha_{11}\Delta T \tag{22}$$

$$\tau_{xz} = Q_{55}(z)\left(\theta_x + \frac{\partial w_0}{\partial x}\right) - e_{15}\left(\frac{\partial \psi(x,t)}{\partial x} cos(\frac{\pi \bar{z}}{h_p})\right) - q_{15}\left(\frac{\partial \phi(x,t)}{\partial x} cos(\frac{\pi \bar{z}}{h_p})\right) \tag{23}$$

In order to extract the governing equations of motion for a sandwich micro beam, in the absence of external force, we assume the Hamilton's principle as follows

$$\int_{t_1}^{t_2} (\delta T - \delta U)\, dt = 0 \tag{24}$$

where T and U represent the total kinetic and strain energies, respectively. δ indicates the variational operator and t shows the time coordinate which differs between the terms t_1 and t_2. The sandwich beam total kinetic energy T can be expressed as Ma *et al*. (2008)

$$T = \frac{1}{2}\int \rho.(\frac{\partial u_i}{\partial t})^2 dz dA \tag{25}$$

By substituting the displacement field into Eq. (25), the kinetic energy can be written as Bamdad *et al*. (2019)

$$T = \frac{1}{2}\int [I_0 (\frac{\partial {u_0}^2}{\partial t} + \frac{\partial {w_0}^2}{\partial t}) + 2I_1(\frac{\partial u_0}{\partial t}.\frac{\partial \theta_x}{\partial t}) + I_2(\frac{\partial \theta_x}{\partial t})^2] dx \tag{26}$$

in which

$$\begin{cases} I_0 = \int_{-\frac{h_c}{2}-hp_1}^{-\frac{h_c}{2}} \rho_f\, dz + \int_{-\frac{h_c}{2}}^{\frac{h_c}{2}} \rho_c dz + \int_{\frac{h_c}{2}}^{\frac{h_c}{2}+hp_2} \rho_f\, dz \\ I_1 = \int_{-\frac{h_c}{2}-hp_1}^{-\frac{h_c}{2}} \rho_f.z\, dz + \int_{-\frac{h_c}{2}}^{\frac{h_c}{2}} \rho_c.z dz + \int_{\frac{h_c}{2}}^{\frac{h_c}{2}+hp_2} \rho_f.z\, dz \\ I_2 = \int_{-\frac{h_c}{2}-hp_1}^{-\frac{h_c}{2}} \rho_f.z^2\, dz + \int_{-\frac{h_c}{2}}^{\frac{h_c}{2}} \rho_c.z^2 dz + \int_{\frac{h_c}{2}}^{\frac{h_c}{2}+hp_2} \rho_f.z^2\, dz \end{cases} \tag{27}$$

I_0, I_1 and I_2 are inertia components of a sandwich micro beam made of porous core and graphene platelets face sheets. ρ_f and ρ_c are mass density of graphene platelets and core, respectively. By applying variational operator to Eq. (26) and simplifying the obtained equations, the variation of total kinetic energy is obtained as

$$\delta T = -\int \left(\left[I_0\frac{\partial^2 u_0}{\partial t^2} + I_1\frac{\partial^2 \theta_x}{\partial t^2}\right]\delta u_0 + \left[I_1\frac{\partial^2 u_0}{\partial t^2} + I_2\frac{\partial^2 \theta_x}{\partial t^2}\right]\delta\theta_x + [I_0\frac{\partial^2 w_0}{\partial t^2}]\delta w_0\right) dx \tag{28}$$

The strain energy of a sandwich micro beam can be written as

$$U = \frac{1}{2}\int \left(\sigma_{ij}\varepsilon_{ij} - D_i E_i - B_i H_i + p_i\gamma_i + \tau_{ijk}\eta_{ijk} + m_{ij}\chi_{ij}\right) dV \tag{29}$$

The variational strain energy for a sandwich micro Timoshenko beam can be written as follows

$$\delta U = \int_V (\sigma_{xx}\delta\varepsilon_{xx} + 2\sigma_{xz}\delta\varepsilon_{xz} - D_1\delta E_1 - D_3\delta E_3 - B_1\delta H_1 - B_3\delta H_3 + \tau_{111}\delta\eta_{111} + \tau_{333}\delta\eta_{333} + 3\tau_{223}\delta\eta_{223} + 6\tau_{221}\delta\eta_{221} + 3\tau_{113}\delta\eta_{113} + + 2m_{12}\chi_{12} + p_1\gamma_1 + p_3\gamma_3) dV \tag{30}$$

where χ_{ij} and η_{ijk} are symmetric gradient rotation and deviator stretch gradient tensors, respectively, γ_i is dilatation gradient vector. τ_{ijk} and m_{ij} are higher order stress tensor. The implied vectors and tensors are specified as (Mohammadimehr and Mostafavifar 2016)

$$\begin{cases} p_i = 2\mu(z){l_0}^2\gamma_i \\ m_{ij} = 2\mu(z){l_2}^2\chi_{ij} \\ \tau_{ijk} = 2\mu(z){l_1}^2\eta_{ijk} \end{cases} \tag{31}$$

in which

$$\begin{cases} \eta_{ijk} = \eta^s_{ijk} - \dfrac{1}{5}(\delta_{ij}\eta^s_{mmk} + \delta_{jk}\eta^s_{mmi} + \delta_{ki}\eta^s_{mmj}) \\ \eta^s_{ijk} = \dfrac{1}{3}(\dfrac{\partial^2 u_i}{\partial x_j \partial x_k} + \dfrac{\partial^2 u_j}{\partial x_i \partial x_k} + \dfrac{\partial^2 u_k}{\partial x_j \partial x_i}) \\ \chi_{ij} = \dfrac{1}{2}(e_{ipq}\varepsilon_{qj,x_p} + e_{jpq}\varepsilon_{qi,x_p}) \\ \gamma_i = \varepsilon_{kk,x_i} \end{cases} \tag{32}$$

And l_0, l_1 and l_2 are defined as three material length scale parameters. Kronecker delta is defined as δ_{ij}, e_{ipq} is permutation symbol and partial derivative component is defined as ",". By investigating and substituting strain components into Eq. (31), higher order strain and stress tensors will be obtained as

$$\begin{cases} p_1 = 2\mu(z) l_0^2 \left(\dfrac{\partial^2 u_0}{\partial x^2} + z\dfrac{\partial^2 \theta_x}{\partial x^2}\right) \\ p_2 = 0 \\ p_3 = 2\mu(z) l_0^2 \left(\dfrac{\partial \theta_x}{\partial x}\right) \end{cases} \tag{33}$$

$$\chi_{12} = \frac{1}{4}\left(\frac{\partial \theta_x}{\partial x} - \frac{\partial^2 w_0}{\partial x^2}\right) \tag{34}$$

$$\begin{cases} \tau_{111} = \dfrac{4}{5}\mu(z) l_1^2 \left(\dfrac{\partial^2 u_0}{\partial x^2} + z\dfrac{\partial^2 \theta_x}{\partial x^2}\right) \\ \tau_{113} = \tau_{131} = \tau_{311} = \dfrac{8}{15}\mu(z) l_1^2 \left(2\dfrac{\partial \theta_x}{\partial x} + \dfrac{\partial^2 w_0}{\partial x^2}\right) \\ \tau_{133} = \tau_{331} = \tau_{313} = \tau_{122} = \tau_{221} = \tau_{212} \\ \quad = -\dfrac{2}{5}\mu(z) l_1^2 \left(\dfrac{\partial^2 u_0}{\partial x^2} + z\dfrac{\partial^2 \theta_x}{\partial x^2}\right) \\ \tau_{322} = \tau_{223} = \tau_{232} = \dfrac{-2}{15}\mu(z) l_1^2 \left(2\dfrac{\partial \theta_x}{\partial x} + \dfrac{\partial^2 w_0}{\partial x^2}\right) \\ \tau_{333} = \dfrac{-2}{5}\mu(z) l_1^2 \left(2\dfrac{\partial \theta_x}{\partial x} + \dfrac{\partial^2 w_0}{\partial x^2}\right) \end{cases} \tag{35}$$

$$\begin{cases} \eta_{111} = \dfrac{2}{5}\left(\dfrac{\partial^2 u_0}{\partial x^2} + z\dfrac{\partial^2 \theta_x}{\partial x^2}\right) \\ \eta_{113} = \eta_{131} = \eta_{311} = \dfrac{4}{15}\left(2\dfrac{\partial \theta_x}{\partial x} + \dfrac{\partial^2 w_0}{\partial x^2}\right) \\ \eta_{133} = \eta_{331} = \eta_{313} = \eta_{122} = \eta_{221} = \eta_{212} \\ \quad = -\dfrac{2}{5}\left(\dfrac{\partial^2 u_0}{\partial x^2} + z\dfrac{\partial^2 \theta_x}{\partial x^2}\right) \\ \eta_{322} = \eta_{223} = \eta_{232} = \dfrac{-1}{15}\left(2\dfrac{\partial \theta_x}{\partial x} + \dfrac{\partial^2 w_0}{\partial x^2}\right) \\ \eta_{333} = \dfrac{-1}{5}\left(2\dfrac{\partial \theta_x}{\partial x} + \dfrac{\partial^2 w_0}{\partial x^2}\right) \end{cases} \tag{36}$$

After obtaining stress components and substituting those into Eq. (30), the variation of strain energy for a sandwich micro beam is written as

$$\begin{aligned} \delta U = \int \{ & \left[\frac{-dN_{xx}}{dx} + \frac{d^2 N_1}{dx^2} + \frac{2}{5}\frac{d^2 N_{111}}{dx^2} - \frac{6}{5}\frac{d^2 N_{221}}{dx^2}\right]\delta u_0 \\ & + \left[\frac{-dM_{xx}}{dx} + N_{xz} + \frac{d^2 M_1}{dx^2} + \frac{2}{5}\frac{d^2 M_{111}}{dx^2} + \frac{2}{5}\frac{dN_{333}}{dx} - \frac{6}{5}\right. \\ & \left.\frac{d^2 M_{221}}{dx^2} + \frac{6}{15}\frac{dN_{223}}{dx} - \frac{dN_3}{dx} - \frac{1}{2}\frac{dM_{12}^{\chi}}{dx} - \frac{24}{15}\frac{dN_{113}}{dx}\right]\delta\theta_x \\ & + \left[-\frac{dN_{xz}}{dx} - \frac{1}{5}\frac{d^2 N_{333}}{dx^2} + \frac{12}{15}\frac{d^2 N_{113}}{dx^2} - \frac{1}{5}\frac{d^2 N_{223}}{dx^2} - \frac{1}{2}\times\right. \\ & \left.\frac{d^2 M_{12}^{\chi}}{dx^2}\right]\delta w_0 + \left[\frac{d\bar{D}_1}{dx} + \bar{D}_3\right]\delta\psi + \left[\frac{d\bar{B}_1}{dx} + \bar{B}_3\right]\delta\phi\}dA \end{aligned} \tag{37}$$

where the resultant force and moment and resultant higher-order force and moment based on modified strain gradient theory are defined as follows

$$\begin{aligned} N_i &= \int p_i dz, M_i = \int p_i . z dz \\ N_{qr} &= \int \sigma_{qr} dz, M_{qr} = \int \sigma_{qr} . z dz \\ N_{ijk} &= \int \tau_{ijk} dz, M_{ijk} = \int \tau_{ijk} . z dz \\ M_{12}^{\chi} &= \int m_{12} dz \end{aligned} \tag{38}$$

in which p_i, τ_{ijk} and m_{12} are obtained from Eqs. (31) and (32). Indices q and r are used for x and y direction and (i, j, k) are equal to 1, 2, 3. By substituting Eqs. (28) and (37) into Eq. (24) and ordering the variables as δu_0, $\delta\theta_x$, δw_0, $\delta\psi$ and $\delta\phi$ coefficients, the governing equations of motion for a sandwich micro beam are obtained as follows

$$\begin{aligned} \delta u_0 : & -A_1\frac{d^2 u_0}{dx^2} - A_2\frac{d^2\theta_x}{dx^2} - A_3\frac{d\psi_0}{dx} - A_4\frac{d\psi(x,t)}{dx} \\ & -A_5\frac{d\phi_0}{dx} - A_6\frac{d\phi(x,t)}{dx} - A_7\frac{d\Delta T}{dx} + 2({l_0}^2.\frac{d^4 u_0}{dx^4}.j^{(0)} \\ & + {l_0}^2.\frac{d^4\theta_x}{dx^4}.j^{(1)}) + \frac{4}{5}({l_1}^2.\frac{d^4 u_0}{dx^4}.j^{(0)} + {l_1}^2.\frac{d^4\theta_x}{dx^4}.j^{(1)}) \\ & = -I_0\frac{\partial^2 u_0}{\partial t^2} - I_1\frac{\partial^2\theta_x}{\partial t^2} \end{aligned} \tag{39}$$

$$\begin{aligned} \delta\theta_x : & -(A_2\frac{d^2 u_0}{dx^2} + A_8\frac{d^2\theta_x}{dx^2} + A_{11}\frac{d\psi_0}{dx} + A_{10}\frac{d\psi(x,t)}{dx} \\ & + A_9\frac{d\phi_0}{dx} + A_{12}\frac{d\phi(x,t)}{dx} + A_{13}\frac{d\Delta T}{dx}) + A_{14}(\theta_x + \frac{\partial w_0}{\partial x}) \\ & - A_{15}\frac{\partial\psi(x,t)}{\partial x} - A_{16}\frac{\partial\phi(x,t)}{\partial x} + 2\left({l_0}^2.\left(\frac{d^4 u_0}{dx^4}\right).j^{(1)}\right. \\ & \left. + {l_0}^2.\left(\frac{d^4\theta_x}{dx^4}\right).j^{(2)}\right) + \frac{4}{5}\left({l_1}^2.\frac{d^4 u_0}{dx^4}.j^{(1)} + {l_1}^2.\frac{d^4\theta_x}{dx^4}.j^{(2)}\right) \\ & - \frac{16}{15}{l_1}^2\left(2\frac{d^2\theta_x}{dx^2} + \frac{d^3 w_0}{dx^3}\right).j^{(0)} - 2{l_0}^2.\frac{d^2\theta_x}{dx^2}.j^{(0)} - \frac{1}{4}{l_2}^2. \\ & (\frac{d^2\theta_x}{dx^2} - \frac{d^3 w_0}{dx^3}).j^{(0)} = -I_1\frac{\partial^2 u_0}{\partial t^2} - I_2\frac{\partial^2\theta_x}{\partial t^2} \end{aligned} \tag{40}$$

$$\begin{aligned} \delta w_0 : & -\left(A_{14}\left(\frac{d\theta_x}{dx} + \frac{\partial^2 w_0}{\partial x^2}\right) - A_{15}\frac{\partial^2\psi}{\partial x^2} - A_{16}\frac{\partial^2\phi}{\partial x^2}\right) + \frac{8}{15} \\ & {l_1}^2\left(2\frac{d^3\theta_x}{dx^3} + \frac{d^4 w_0}{dx^4}\right).j^{(0)} - \frac{1}{4}{l_2}^2\left(\frac{d^3\theta_x}{dx^3} - \frac{d^4 w_0}{dx^4}\right).j^{(0)} \\ & = -I_0\frac{\partial^2 w_0}{\partial t^2} \end{aligned} \tag{41}$$

$$\begin{aligned} \delta\psi : & A_{17}\left(\frac{d\theta_x}{dx} + \frac{d^2 w_0}{dx^2}\right) + A_{18}\frac{d^2\psi}{dx^2} + A_{19}\frac{d^2\phi}{dx^2} + A_4\frac{du_0}{dx} \\ & + A_{10}\frac{d\theta_x}{dx} - A_{20}\psi_0 - A_{21}\psi(x,t) - A_{22}\phi_0 - A_{23}\phi(x,t) \\ & = 0 \end{aligned} \tag{42}$$

$$\begin{aligned} \delta\phi : & A_{24}\left(\frac{d\theta_x}{dx} + \frac{d^2 w_0}{dx^2}\right) + A_{25}\frac{d^2\psi}{dx^2} + A_{26}\frac{d^2\phi}{dx^2} + A_6\frac{du_0}{dx} \\ & + A_{12}\frac{d\theta_x}{dx} - A_{22}\psi_0 - A_{23}\psi(x,t) - A_{27}\phi_0 - A_{28}\phi(x,t) \\ & = 0 \end{aligned} \tag{43}$$

Table 1 The validation of first three natural frequencies for sandwich beam for simply-support boundary conditions and uniform distribution (V^*_{CNT} = 0.12, h_c = 0.08, h_f = 0.01 and L = 20h)

Mode number	Present study	Chen *et al.* (2016)	% Error
1	0.1384	0.1432	3.35
2	0.5405	0.5650	4.34
3	1.1825	1.2429	4.86

Table 2 Material characteristics of GPL

Young's modulus (GPa)	1010
Density (kg m^{-3})	1062.5
Poisson's ratio	0.186
Thermal coefficient (× 10^{-6}/K)	5.0

4. Solution method

In this section, the solution method for the porous sandwich beam with two piezo magnetoelectric face sheets in a thermal environment will be studied. The Navier's type method is considered to solve the differential equations of motion. For simply supported boundary conditions, we have

$$\frac{\partial u_0}{\partial x} = 0, \quad \frac{\partial \theta_x}{\partial x} = 0, \quad \frac{\partial^2 w_0}{\partial x^2} = 0 \quad w_0 = 0 \quad \text{at } x = 0, L \tag{44a}$$

$$\begin{cases} u_{0(x,t)} = \sum u_n \cos(\lambda_n x)\, e^{i\omega t} \\ \theta_{x(x,t)} = \sum \theta_n \cos(\lambda_n x)\, e^{i\omega t} \\ W_{0(x,t)} = \sum W_n \sin(\lambda_n x) e^{i\omega t} \\ \phi_{(x,t)} = \sum \phi_n \sin(\lambda_n x) e^{i\omega t} \\ \psi_{(x,t)} = \sum \psi_n \sin(\lambda_n x) e^{i\omega t} \end{cases} \tag{44b}$$

where $\lambda_n = \frac{n\pi}{L}$, i is assumed $\sqrt{-1}$, u_n, θ_n, w_n, ϕ_n and ψ_n are unknown coefficients, and ω is the natural frequency of the system. For deriving the mass and stiffness matrices, we substitute Eq. (44) into Eqs. (39)-(43) that is defined as follows

$$([K] - S[M])\{X\} = \{0\} \tag{45}$$

in which M and K are stiffness and mass matrices, respectively, S is equal to ω^2 and X is displacement parameters.

5. Results and discussion

5.1 Validation and reliability

To validate the obtained results from the present study and Chen *et al.* (2016a, b), the physical and geometrical characteristics for homogenous core (Ti-6A1-4V) are ρ_{core} = 4430 (kg/m^3), v_{core} = 0.342 and E_{core} = 113.8 (GPa). The composite face sheet layers for material constants are ρ_{CNT} = 1400 (kg/m^3), E_m = 2.5 (GPa), E_{CNT} = 5.6466 (TPa), v_{CNT} = 0.175, v_m = 0.3, V^*_{CNT} = 0.12 and ρ_m = 1190 (kg/m^3), where CNT and m refer to carbon nanotube and matrix, respectively. Table 1 compares the first three natural frequencies by the present work and the obtained results by Chen *et al.* (2016a) for simply-support boundary conditions and uniform porous distribution. It can be seen from this table that there is a good agreement between them.

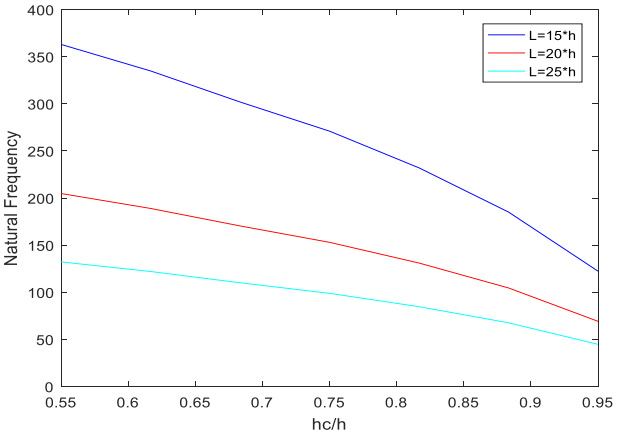

Fig. 4 Natural frequency versus h_c/h for different aspect ratio (L/h)

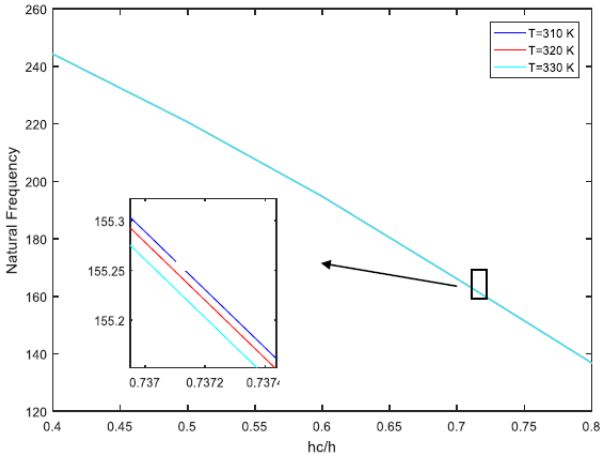

Fig. 5 Natural frequency of sandwich beam with uniform porous distribution in terms of h_c/h for different value of temperature

5.2 Numerical results

In this study, the effects of different parameters including porosity parameters, magnetic and electric coefficients, porosity coefficient, graphene platelets parameters, and the geometrical constants on natural frequency are discussed. The following characteristics are assumed for this case: L = 20h, T_0 = 300K, $l_0 = l_1 = l_2$ = 17.6 nm, η_1 = 0.137, η_3 = 0.715, e_{31} = −2.2, q_{31} = 290.1, e_{15} = 5.8,

Table 3 Natural frequency of the beam in different temperature for various porous distributions ($e_0 = 0.2$, $L = 20h$, $W_{GPL} = 4\%$)

Various distributions of porous core	Natural frequency ($\times 10^2$)		
	T = 310 (K)	T = 320 (K)	T = 330 (K)
D1	2.459989458471953	2.459972825149710	2.459945747392724
	2.222766857594586	2.222736388849169	2.222686787650810
	1.962502939978166	1.962451217770869	1.962367015887891
	1.674164898062112	1.674079921811244	1.673941579135663
D2	2.443295967700836	2.443278958462255	2.443251268736507
	2.206737714752794	2.206706568929398	2.206655865465498
	1.947737139379540	1.947684282475240	1.947598233261747
	1.661172816557279	1.661085994909007	1.660944647621665
D3	2.443293796263445	2.443277152150807	2.443250088720874
	2.206733041499421	2.206702601997906	2.206653048401067
	1.947728200027966	1.947675322931420	1.947592419005284
	1.661156420517487	1.661071554337251	1.660933390630535

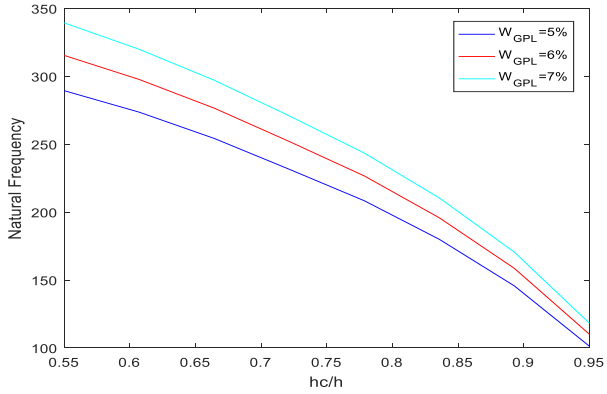

Fig. 6 The effect of W_{GPL} increment on the natural frequency

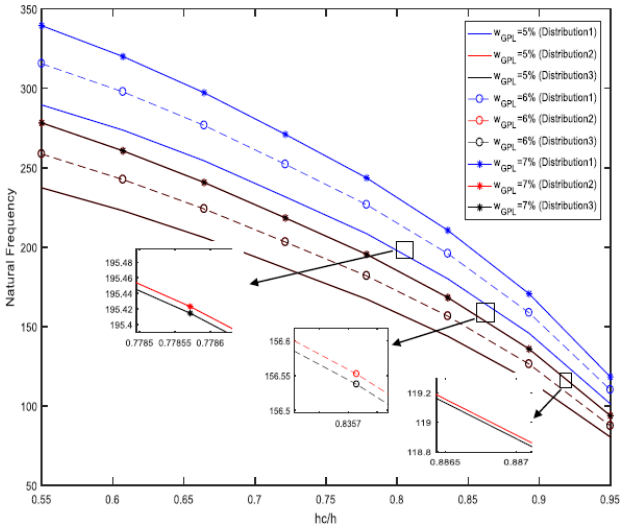

Fig. 7 The effect of different porous distributions on the natural frequency for various W_{GPL}

$q_{15} = 275$, $g_{11} = 5.367 \times 10^{-12}$, $g_{33} = 2737.5 \times 10^{-12}$, $\eta_{11} = 5.64 \times 10^{-9}$, $\eta_{33} = 6.35 \times 10^{-9}$, $\mu_{11} = -297 \times 10^{-6}$, $\mu_{33} = 83.5 \times 10^{-6}$, $\rho_f = 10^3$, $E_{GPL} = 1010$ GPa, $\rho_m = 1200$, $\rho_{GPL} = 1062.5$, $v_m = 0.3$, $v_{GPL} = 0.186$, $a_{GPL} = 2.5$ μm, $b_{GPL} = 1.5$ μm, $t_{GPL} = 1.5$ μm.

The material properties of graphene platelets (GPLs) are indexed in Table 2 as follows (Wu *et al*. 2017).

Fig. 4 shows the natural frequency versus thickness ratio (h_c/h). It is understood that with an increase in aspect ratio (L/h), the natural frequency diminishes. It is seen that increasing aspect ratio leads to decrease the stiffness of micro beam, and then the natural frequency reduces.

It can also be found from Fig. 5 that with increasing of the temperature change, the stiffness of core and face layers decreases and as a result, the natural frequency diminishes.

Table 3 shows the natural frequency of the beam in different temperature for various porous distributions. In Fig. 5 and Table 3, it is seen that increasing the temperature change leads to decrease the natural frequency because the micro beam becomes softer. On the other hands, as the temperature change enhances, the micro structure becomes more flexible and the intermolecular bonds decrease. It can be seen from this figure that the natural frequency for T = 310K, h_c/h = 0.6, is 0.08% and 0.2% more than for T = 320K and T = 330K, respectively.

Table 4 illustrates the natural frequency of beam in various porous distributions. According to the results, it can be seen that for all porous distributions, with increasing of porosity coefficient, the natural frequency increases. Also, it is shown that distribution 1 has the most value of the natural frequency and distribution 3 owns the least. In Table 4, it is seen that by increasing porosity coefficient, the natural frequency increases because both stiffness and mass matrices decreases, but the effect of reduction of mass matrix is more than stiffness matrix.

Fig. 6 illustrates the effect of volume fraction of GPL on the natural frequency. It can see that with increasing of the value of W_{GPL}, the stiffness of microbeam increases. As a result, the amount of natural frequency enhances. It is shown from Fig. 6 that in h_c/h = 0.7, the natural frequency for W_{GPL} = 0.05 is 8% and 14% less than its for W_{GPL} = 0.06 and W_{GPL} = 0.07, respectively.

The effect of different porous distributions on the natural frequency of sandwich beam for different W_{GPL} is shown in Fig. 7. As can be figured out, distribution 1 has the maximum amount of natural frequency, and distribution

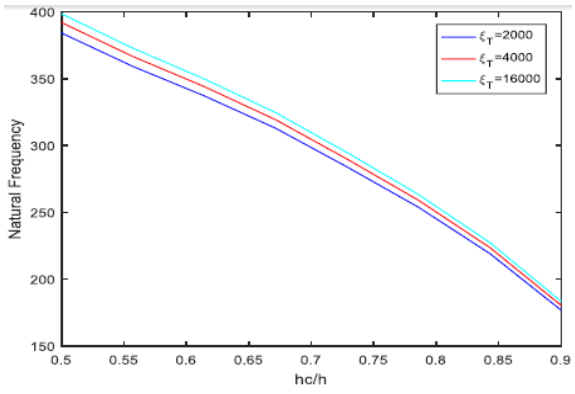

(a)

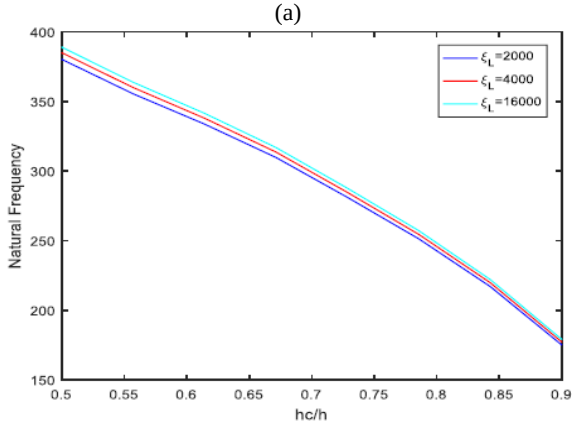

(b)

Fig. 8 The natural frequency of sandwich beam in terms of h_c/h for different values of (a) ξ_T and (b) ξ_L

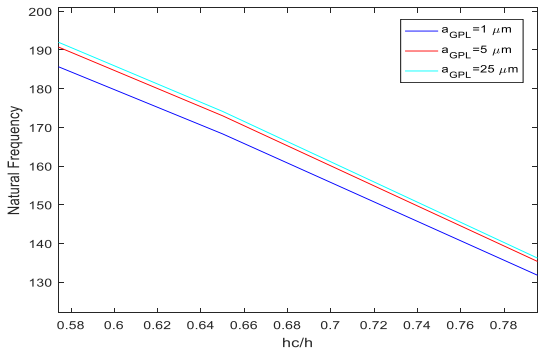

Fig. 9 The effect of a_{GPL} changes on the natural frequency

3 contains the minimum one. It can be seen that by increasing the thickness ratio (h_c/h), the natural frequency decreases because the material properties of core are lower than it's for face sheets layers. It can be seen that for the ratio of h_c/h = 7 and W_{GPL} = 0.05, the natural frequency for distribution 1 is 18% and 20% more than the one for distributions 2 and 3, respectively. It is also presented that for distribution1, when the ratio of h_c/h = 0.7, the natural frequency for W_{GPL} = 0.07 denote 7% and 15% more than the one for W_{GPL} = 0.06 and W_{GPL} = 0.05, respectively.

Figs. 8(a) and (b) display the natural frequency of the sandwich beam versus thickness ratio (h_c/h). It is seen that with increasing the value of ξ_L, ξ_T the amount of the natural frequency increases because the stiffness of micro-

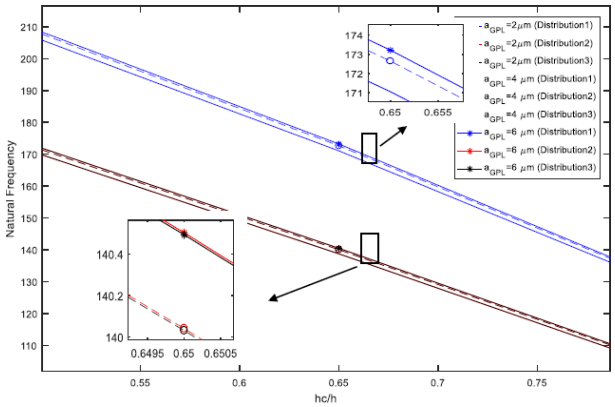

Fig. 10 The effect of different porous distributions on the natural frequency in terms of h_c/h for a_{GPL} = 2 μm, 4 μm, 6 μm

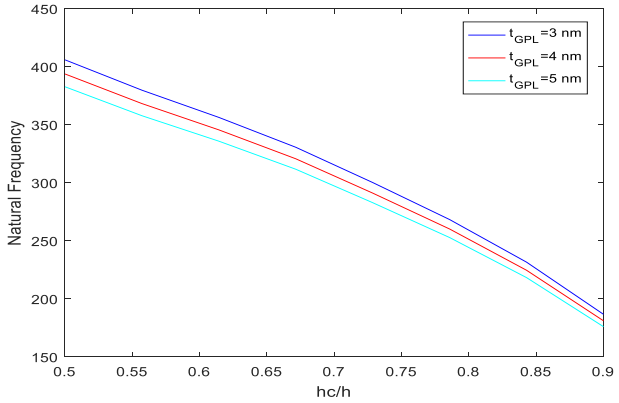

Fig. 11 The increment of GPL thickness effects on natural frequency of sandwich beam

structures increases. It can be seen from Fig. 8(a) that the natural frequency for ξ_T = 16000 and h_c/h = 0.7 is 1.6% and 3.6% more than the one for ξ_T = 4000 and ξ_T = 2000, respectively. It is shown from Fig. 8(b) that the natural frequency for ξ_L = 16000 and h_c/h = 0.7 is 1.2% and 2.2% more than the one for ξ_L = 4000 and ξ_L = 2000, respectively.

In Fig. 9, the influence of a_{GPL} changes on the natural frequency of the beam is indicated. The results show that with an increment in the a_{GPL}, the natural frequency increases because the stiffness of micro structures enhances. It can be seen that the natural frequency for a_{GPL} = 25 μm and h_c/h = 0.6 is 0.3% and 1% more than the one for a_{GPL} = 5 μm and a_{GPL} = 1 μm, respectively.

The effect of different porous distributions on the natural frequency for different a_{GPL} is shown in Fig. 10. The results reveal that distribution 1 has the highest natural frequency value and the natural frequencies which extracted from distributions 2 and 3 are very close to each other. The results illustrate that with an increase in the value of a_{GPL}, the natural frequency increases because the stiffness of micro structures enhances. It is shown that the natural frequency for distribution 1, h_c/h = 0.7 and a_{GPL} = 6 μm is 19% and 20% more than the one for distribution 2 and 3, respectively.

The effect of GPL thickness on the natural frequency is

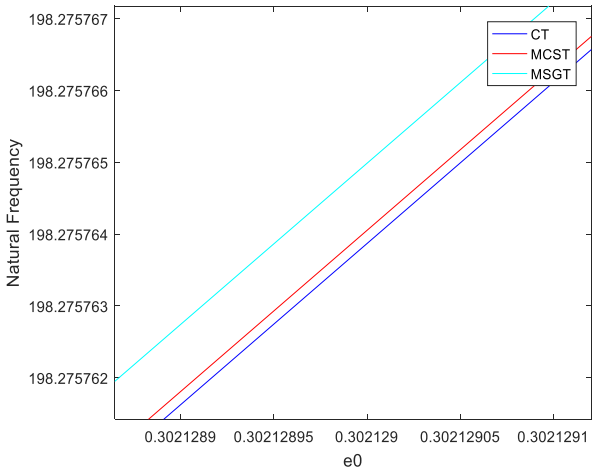

Fig. 12 The effects of various size dependent theories including CT, MCST and MSGT on natural frequency

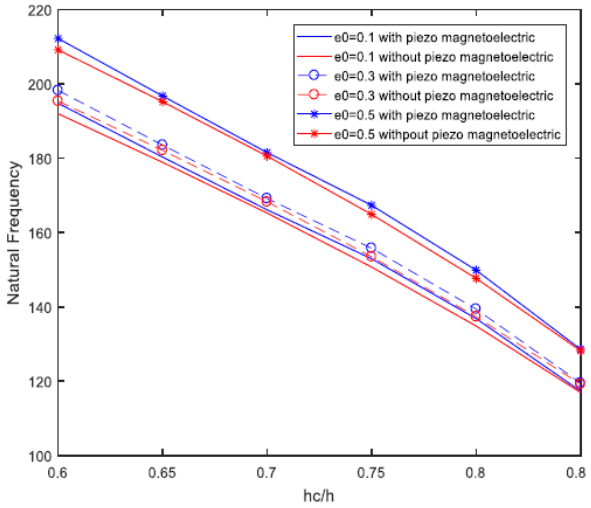

Fig. 13 The effects of piezo magneto electric layers on the natural frequency

investigated and illustrated in Fig. 11. As can be seen, with increasing of the value of GPL thickness, the natural frequency decreases because the micro beam becomes softer.

Fig. 12 illustrates the effect of different theories such as CT, MCST and MSGT. It reveals that MSG theory owns the most value of the natural frequency, and the least of it is for classical theory because modified strain gradient and modified couple stress theories consider three and one material length scale parameters, respectively while classical theory does not consider any material length scale parameter. Thus, the stiffness of a micro beam by considering three material length scale parameters is higher than other theories and then the natural frequency is more.

Fig. 13 shows the effects of piezo magneto electric layers on the natural frequency. It is seen that the natural frequency with considering the piezo magneto-electric layers is higher than that of without considering its. It is seen that by increasing porosity coefficient, the natural frequency increases because both stiffness and mass matrices decreases, but the effect of reduction of mass matrix is more than stiffness matrix. Considering the piezo magneto-electric layers lead to enhance the stiffness of a micro beam, thus the natural frequency increases.

6. Conclusions

In this article, the free vibration analysis of electro-magneto-thermo sandwich Timoshenko beam made of porous core and GPLRC using MSGT is investigated. The present beam is considered as magneto-electro-elastic and composite reinforced by graphene platelets in face sheets layers and a porous core that the material properties are dependent on temperature changes. The governing equations of motion are derived by using Hamilton's principle. The effects of various parameters such as one and three material length scale parameters, temperature change, various distributions of the porous, different volume fraction of graphene platelets and ratio of core to face thickness on the natural frequency of Timoshenko sandwich beam are considered. It is seen that increasing aspect ratio leads to decrease the stiffness of micro beam, and then the natural frequency decreases. It can see that increasing the temperature change leads to decrease the natural frequency because the micro beam becomes softer. On the other hands, as the temperature change enhances, the micro structure becomes more flexible and the intermolecular bonds decrease. It can be seen from this figure that the natural frequency for T = 310K, h_c/h = 0.6 is 0.08% and 0.2 % more than for T = 320K and T = 330K, respectively. It can be seen that with increasing of the value of W_{GPL}, the stiffness of microbeam increases. As a result, the amount of natural frequency enhances. It is shown from this figure that in h_c/h = 0.7, the natural frequency for W_{GPL} = 0.05 is 8% and 14% less than its for W_{GPL} = 0.06 and W_{GPL} = 0.07, respectively. It can be seen that the distributions 1 and 3 have the maximum and minimum amount of the natural frequency, respectievly. It is shown that by increasing the thickness ratio (h_c/h), the natural frequency decreases because the material properties of core are lower than it's for face sheets layers. It can be seen that for the ratio of h_c/h = 0.7 and W_{GPL} = 0.05, the natural frequency for distribution 1 is 18% and 20% more than the one for distributions 2 and 3, respectively. It is also presented that for distribution1, when the ratio of h_c/h = 0.7, the natural frequency for W_{GPL} = 0.07 denote 7% and 15% more than the one for W_{GPL} = 0.06 and W_{GPL} = 0.05, respectively. It is seen that with increasing the value of ξ_L, ξ_T, the amount of the natural frequency increases because the stiffness of micro structures increases. It can be seen from the figure that the natural frequency for ξ_T = 16000 and h_c/h = 0.7 is 1.6% and 3.6% more than the one for ξ_T = 4000 and ξ_T = 2000, respectively. It is shown that the natural frequency for ξ_L = 16000 and h_c/h = 0.7 is 1.2% and 2.2% more than the one for ξ_L = 4000 and ξ_L = 2000, respectively. The results show that with an increment in the length and width of GPLs, the natural frequency increases because the stiffness of micro structures enhances and vice versa for thickness of GPLs. It

can be seen that the natural frequency for a_{GPL} = 25 μm and h_c/h = 0.6 is 0.3% and 1% more than the one for a_{GPL} = 5 μm and a_{GPL} = 1 μm, respectively. It is shown that MSGT and CT have the most and lowest values of the natural frequency, because modified strain gradient and modified couple stress theories consider three and one material length scale parameters, respectively while classical theory does not consider any material length scale parameter. Thus, the stiffness of a micro beam by considering three material length scale parameters is higher than other theories and then the natural frequency is more. It is seen that the natural frequency with considering the piezo magneto-electric layers is higher than that of without considering its. It is seen that by increasing porosity coefficient, the natural frequency increases because both stiffness and mass matrices decreases, but the effect of reduction of mass matrix is more than stiffness matrix. Considering the piezo magneto-electric layers lead to enhance the stiffness of a micro beam, thus the natural frequency increases.

Acknowledgments

The authors would like to thank the reviewers for their valuable comments and suggestions to improve the clarity of this work. Also, they would like to acknowledgement the Iranian Nanotechnology Development Committee for supporting this research and the University of Kashan under Grant No. 8911238/25.

References

AkhavanAlavi, S.M., Mohammadimehr, M. and Edjtahed, S.H. (2019), "Active control of micro Reddy beam integrated with functionally graded nanocomposite sensor and actuator based on linear quadratic regulator method", *Eur. J. Mech. A Solids*, **74**, 449-461. https://doi.org/10.1016/j.euromechsol.2018.12.008.

Arefi, M. and Zenkour A.M. (2017), "Vibration and bending analysis of a sandwich microbeam with two integrated piezo-magnetic face-sheets", *Compos. Struct.*, **159**, 479-490. https://doi.org/10.1080/01495739.2016.1229146

Arshid, E. and Khorshidvand, A.R. (2018), "Free vibration analysis of saturated porous FG circular plates integrated with piezoelectric actuators via differential quadrature method", *Thin-Wall. Struct.*, **125**, 220-233. https://doi.org/10.1016/j.tws.2018.01.007.

Babaeeian, M. and Mohammadimehr, M. (2020), "Investigation of the time elapsed effect on residual stress measurement in a composite plate by DIC method", *Opt. Lasers Eng.*, **128**, 106002. https://doi.org/10.1016/j.optlaseng.2020.106002.

Bahaadini, R. and Saidi, A.R. (2018), "Aeroelastic analysis of functionally graded rotating blades reinforced with graphene nanoplatelets in supersonic flow", *Aerosp. Sci. Technol.*, **80**, 381-391. https://doi.org/10.1016/j.ast.2018.06.035.

Bamdad, M., Mohammadimehr, M. and Alambeigi, K. (2019), "Analysis of sandwich Timoshenko porous beam with temperature-dependent material properties: Magneto-electro-elastic vibration and buckling solution", *J. Vib. Control*, **25**(23-24), 2875-2893. https://doi.org/10.1177/1077546319860314.

Barati, M.R. and Shahverdi, H. (2019), "Finite element forced vibration analysis of refined shear deformable nanocomposite graphene platelet-reinforced beams", *J. Braz. Soc. Mech. Sci. Eng.*, **42**(1), 33-48. https://doi.org/10.1007/s40430-019-2118-8.

Chen, D., Yang, J. and Kitipornchai S. (2015), "Elastic buckling and static bending of shear deformable functionally graded porous beam", *Compos. Struct.*, **133**, 54-61. https://doi.org/10.1016/j.compstruct.2015.07.052.

Chen, D., Kitipornchai, S. and Yang, J. (2016a), "Nonlinear free vibration of shear deformable sandwich beam with a functionally graded porous core", *Thin-Wall. Struct.*, **107**, 39-48. https://doi.org/10.1016/j.tws.2016.05.025.

Chen, D., Yang, J. and Kitipornchai, S. (2016b), "Free and forced vibrations of shear deformable functionally graded porous beams", *Int. J. Mech. Sci.*, **108-109**, 14-22. https://doi.org/10.1016/j.ijmecsci.2016.01.025.

Chen, S., Hassanzadeh-Aghdam, M.K. and Ansari, R. (2018), "An analytical model for elastic modulus calculation of SiC whisker-reinforced hybrid metal matrix nanocomposite containing SiC nanoparticles", *J. Alloys Compd.* **767**, 632-641. https://doi.org/10.1016/j.jallcom.2018.07.102.

Crupi, V. and Montanini, R. (2007), "Aluminium foam sandwiches collapse modes under static and dynamic three-point bending", *Int. J. Impact Eng.*, **34**(3), 509-521. https://doi.org/10.1016/j.ijimpeng.2005.10.001.

Ebrahimi, F., Kokaba, M.R., Shaghaghi, G.R. and Selvamani, R. (2020), "Dynamic characteristics of hygro-magneto-thermo-electrical nanobeam with non-ideal boundary conditions", *Adv. Nano Res., Int. J.*, **8**(2), 169-182. https://doi.org/10.12989/anr.2020.8.2.169.

Gao, N., Cheng, B., Hou, H. and Zhang, R. (2018), "Mesophase pitch based carbon foams as sound absorbers", *Mater. Lett.*, **212**, 243-246. https://doi.org/https://doi.org/10.1016/j.matlet.2017.10.074.

Gibson, L.J. and Ashby, M.F. (1997), *Introduction Cellular Solids: Structure and Properties*. Cambridge University Press, USA. https://doi.org/10.1017/CBO9781139878326.003.

Grygorowicz, M., Magnucki, K. and Malinowski, M. (2015), "Elastic buckling of a sandwich beam with variable mechanical properties of the core", *Thin-Wall. Struct.*, **87**, 127-132. https://doi.org/10.1016/j.tws.2014.11.014.

Guo, X.Y. and Zhang, W. (2016), "Nonlinear vibrations of a reinforced composite plate with carbon nanotubes", *Compos. Struct.*, **135**, 96-108. https://doi.org/10.1016/j.compstruct.2015.08.063.

Hoang, V.N.V., Minh, V.T., Ninh, D.G., Nguyen, C.T. and Huy, V.L. (2020a), "Effects of non-uniform elastic foundation on the nonlinear vibration of nanocomposite plates in thermal environment using Selvadurai methodology", *Compos. Struct.*, **253**, 112812. https://doi.org/10.1016/j.compstruct.2020.112812.

Hoang, V.N.V., Tien, N.D., Ninh, D.G., Thang, V.T. and Troung, D.V. (2020b), "Nonlinear dynamics of functionally graded graphene nanoplatelet reinforced polymer doubly-curved shallow shells resting on elastic foundation using a micromechanical model", *J. Sandw. Struct. Mater.*, **2020**, 1099636220926650. https://doi.org/10.1177/1099636220926650.

Hosseini, M. and Jamalpoor, A. (2015), "Analytical solution for thermomechanical vibration of double-viscoelastic nanoplate-systems made of functionally graded materials", *J. Therm. Stresses*, **38**(12), 1428-1456. https://doi.org/10.1080/01495739.2015.1073986.

Ma, H.M., Gao, X.L. and Reddy, J.N. (2008), "A microstructure-dependent Timoshenko beam model based on a modified couple stress theory", *J. Mech. Phys. Solids*, **56**(12), 3379-3391. https://doi.org/10.1016/j.jmps.2008.09.007.

Magnuca-Blandzi E. (2011), "Mathematical modelling of a rectangular sandwich plate with a metal foam core", *J. Theor. Appl. Mech.*, **49**(2), 439-455.

Mohammadimehr, M. and Mostafavifar M. (2016), "Free vibration

analysis of sandwich plate with a transversely flexible core and FG-CNTs reinforced nanocomposite face sheets subjected to magnetic field and temperature-dependent material properties using SGT", *Compos. Part B Eng.* **94**, 253-270. https://doi.org/10.1016/j.compositesb.2016.03.030.

Mohammadimehr, M. and Meskini, M. (2020), "Analysis of porous micro sandwich plate: Free and forced vibration under magneto-electro-elastic loadings", *Adv. Nano Res., Int. J.*, **8**(1), 69-82. https://doi.org/10.12989/anr.2020.8.1.069.

Mohammadimehr, M., Rousta Navi, B. and Ghorbanpour Arani, A. (2015a), "Free vibration of viscoelastic double-bonded polymeric nanocomposite plates reinforced by FG-SWCNTs using MSGT, sinusoidal shear deformation theory and meshless method", *Compos. Struct.*, **131**, 654-671. https://doi.org/10.1016/j.compstruct.2015.05.077.

Mohammadimehr, M., Rostami, R. and Arefi, M. (2015b), "Electro-elastic analysis of a sandwich thick plate considering FG core and composite piezoelectric layers on Pasternak foundation using TSDT", *Steel Compos. Struct., Int. J.*, **20**(3), 513-543. https://doi.org/10.12989/scs.2016.20.3.513.

Mohammadimehr, M., Salemi, M. and Rousta Navi, B. (2016), "Bending, buckling, and free vibration analysis of MSGT microcomposite Reddy plate reinforced by FG-SWCNTs with temperature-dependent material properties under hydro-thermo-mechanical loadings using DQM", *Compos. Struct.*, **138**, 361-380. https://doi.org/10.1016/j.compstruct.2015.11.055.

Mohammadimehr, M., Mohammadi-Dehabadi, A.A., Akhavan Alavi, S.M., Alambeigi, K., Bamdad, M., Yazdani, R. and Hanifehlou, S. (2018), "Bending, buckling, and free vibration analyses of carbon nanotube reinforced composite beams and experimental tensile test to obtain the mechanical properties of nanocomposite", *Steel Compos. Struct., Int. J.*, **29**(3), 405-422. https://doi.org/10.12989/scs.2018.29.3.405.

Mohammadimehr, M., Monajemi, A.A. and Afshari, H. (2020), "Free and forced vibration analysis of viscoelastic damped FG-CNT reinforced micro composite beams", *Microsyst. Technol.*, **26**, 3085-3099. https://doi.org/10.1007/s00542-017-3682-4.

Nejadi, M.M. and Mohammadimehr, M. (2020), "Buckling analysis of nano composite sandwich Euler-Bernoulli beam considering porosity distribution on elastic foundation using DQM", *Adv. Nano Res., Int. J.*, **8**(1), 59-68. https://doi.org/10.12989/anr.2020.8.1.059.

Ninh, D.G. (2018), "Nonlinear thermal torsional post-buckling of carbon nanotube-reinforced composite cylindrical shell with piezoelectric actuator layers surrounded by elastic medium", *Thin-Wall. Struct.*, **123**, 528-538. https://doi.org/10.1016/j.tws.2017.11.027.

Ninh, D.G. and Bich, D.H. (2018), "Characteristics of nonlinear vibration of nanocomposite cylindrical shells with piezoelectric actuators under thermo-mechanical loads", *Aerosp. Sci. Technol.*, **77**, 595-609. https://doi.org/10.1016/j.ast.2018.04.008.

Ninh, D.G. and Tien, N.D. (2019), "Investigation for electro-thermo-mechanical vibration of nanocomposite cylindrical shells with an internal fluid flow", *Aerosp. Sci. Technol.*, **92**, 501-519. https://doi.org/10.1016/j.ast.2019.06.023.

Ninh, D.G., Tien, N.D. and Hoang, V.N.V. (2019), "Analyses of nonlinear dynamics of imperfect nanocomposite circular cylindrical shells with swirling annular and internal fluid flow using higher order shear deformation shell theory", *Eng. Struct.*, **198**, 109502. https://doi.org/10.1016/j.engstruct.2019.109502.

Noroozi, R., Barati, A., Kazemi, A., Norouzi, S. and Hadi, A. (2020), "Torsional vibration analysis of bi-directional FG nano-cone with arbitrary cross-section based on nonlocal strain gradient elasticity", *Adv. Nano Res., Int. J.*, **8**(1), 13-24. https://doi.org/10.12989/anr.2020.8.1.013.

Qin, Q.H. and Wang, T.J. (2009), "An analytical solution for the large deflections of a slender sandwich beam with a metallic foam core under transverse loading by a flat punch", *Compos. Struct.*, **88**, 509-518. https://doi.org/10.1016/j.compstruct.2008.05.012.

Rafiee, M., Yang, J. and Kitipornchai, S. (2013), "Large amplitude vibration of carbon nanotube reinforced functionally graded composite beams with piezoelectric layers", *Compos. Struct.*, **96**, 716-725. https://doi.org/10.1016/j.compstruct.2012.10.005.

Rajabi, J. and Mohammadimehr, M. (2019), "Hydro-thermo-mechanical biaxial buckling analysis of sandwich micro-plate with isotropic/orthotropic cores and piezoelectric/polymeric nanocomposite face sheets based on FSDT on elastic foundations", *Steel Compos. Struct., Int. J.*, **33**(4), 509-523. https://doi.org/10.12989/scs.2019.33.4.509.

Shahdin, A., Mezeix, L., Bouvet, C., Morlier, J. and Gourinat, Y. (2009), "Fabrication and mechanical testing of glass fiber entangled sandwich beams: A comparison with honeycomb and foam sandwich beams", *Compos. Struct.*, **90**(4), 404-412. https://doi.org/10.1016/j.compstruct.2009.04.003.

Shen, H.S., Lin, F. and Xiang, Y. (2017), "Nonlinear vibration of functionally graded graphene-reinforced composite laminated beams resting on elastic foundations in thermal environments", *Nonlin. Dyn.* **90**(2), 899-914. https://doi.org/10.1007/s11071-017-3701-0.

Si Tayeb, T., Zidour, M., Bensattalah, T., Heireche, H., Benahmed, A. and Adda Bedia, E.A. (2020), "Mechanical buckling of FG-CNTs reinforced composite plate with parabolic distribution using Hamilton's energy principle", *Adv. Nano Res., Int. J.*, **8**(2), 135-148. https://doi.org/10.12989/anr.2020.8.2.135.

Tagarielli, V.L., Deshpande, V.S. and Fleck, N.A. (2007), "The dynamic response of composite sandwich beams to transverse impact", *Int. J. Solids Struct.* **44**(7), 2442-2457. https://doi.org/10.1016/j.ijsolstr.2006.07.015.

Tien, N.D., Hoang, V.N.V., Ninh, D.G., Huy, V.L. and Hung, N.C. (2020), "Nonlinear dynamics and chaos of a nanocomposite plate subjected to electro-thermo-mechanical loads using Flügge-Lur'e-Bryrne theory", *J. Vib. Control*, **2020**, 1077546320938185. https://doi.org/10.1177/1077546320938185.

Wadley, H.N.G., Fleck, N.A. and Evans, A.G. (2003), "Fabrication and structural performance of periodic cellular metal sandwich structures", *Compos. Sci. Technol.*, **63**(16), 2331-2343. https://doi.org/10.1016/S0266-3538(03)00266-5.

Wang, M., Guo, Y., Wang, B., Luo, H., Zhang, X., Wang, Q., Zhang, Y., Wu, H., Liu, H. and Dou, S. (2020), "An engineered self-supported electrocatalytic cathode and dendrite-free composite anode based on 3D double-carbon hosts for advanced Li-SeS_2 batteries", *J. Mater. Chem. A*, **8**(6), 2969-2983. https://doi.org/10.1039/C9TA11124G.

Wu, H., Kitipornchai, S. and Yang, J. (2015), "Free vibration and buckling analysis of sandwich beams with functionally graded carbon nanotube-reinforced composite face sheets", *Int. J. Struct. Stab. Dyn.*, **15**(7), 1540011. https://doi.org/10.1142/S0219455415400118.

Wu, H., Yang, J. and Kitipornchai, S. (2017), "Dynamic instability of functionally graded multilayer graphene nanocomposite beams in thermal environment", *Compos. Struct.*, **162**, 244-254. https://doi.org/10.1016/j.compstruct.2016.12.001.

Zenkour, A.M. and Arefi, M. (2017), "Nonlocal transient electrothermomechanical vibration and bending analysis of a functionally graded piezoelectric single-layered nanosheet rest on visco-Pasternak foundation", *J. Therm. Stresses*, **40**(2), 1-18. https://doi.org/10.1080/01495739.2016.1229146.

Zeverdejani, M.K. and Beni, Y.T. (2020), "Effect of laminate configuration on the free vibration/buckling of FG Graphene/PMMA composites", *Adv. Nano Res., Int. J.*, **8**(2), 103-114. https://doi.org/10.12989/anr.2020.8.2.103.

Zhang, L.W., Lei, Z.X. and Liew, K.M. (2015), "Free vibration analysis of FG-CNT reinforced composite straight-sided

quadrilateral plates resting on elastic foundations using the IMLS-Ritz method", *J. Vib. Control*, **23**(6), 1026-1043. https://doi.org/10.1177/1077546315587804.

Zhao, H., Li, Y., Song, Q., Liu, S., Ma, Q., Ma, L. and Shu, X. (2019), "Catalytic reforming of volatiles from co-pyrolysis of lignite blended with corn straw over three different structures of iron ores", *J. Anal. Appl. Pyrolysis*, **144**, 104714. https://doi.org/10.1016/j.jaap.2019.104714

Zhao, H., Li, Y., Song, Q., Ma, Q., Ma, L., Liu, S. and Shu, X. (2020), "The rate-limiting step in the integrated coal tar decomposition and upgrading-iron ore reduction reaction determined by kinetic analysis", *J. Anal. Appl. Pyrolysis*, **147**, 104808. https://doi.org/10.1016/j.jaap.2020.104808.

Zhou, H.W., Mishnaevsky, L., Yi, H.Y., Liu, Y.Q., Hu, X., Warrier, A. and Dai, G.M. (2016), "Carbon fiber/carbon nanotube reinforced hierarchical composites: Effect of CNT distribution on shearing strength", *Compos. Part B Eng.*, **88**, 201-211. https://doi.org/10.2514/1.11780.

CC